



## Discovery of new non-pyrimidine scaffolds as *Plasmodium falciparum* DHFR inhibitors by fragment-based screening

Marie Hoarau, Jarunee Vanichtanankul, Nitipol Srimongkolpithak, Danoo Vitsupakorn, Yongyuth Yuthavong & Sumalee Kamchonwongpaisan

To cite this article: Marie Hoarau, Jarunee Vanichtanankul, Nitipol Srimongkolpithak, Danoo Vitsupakorn, Yongyuth Yuthavong & Sumalee Kamchonwongpaisan (2021) Discovery of new non-pyrimidine scaffolds as *Plasmodium falciparum* DHFR inhibitors by fragment-based screening, Journal of Enzyme Inhibition and Medicinal Chemistry, 36:1, 198-206, DOI: [10.1080/14756366.2020.1854244](https://doi.org/10.1080/14756366.2020.1854244)

To link to this article: <https://doi.org/10.1080/14756366.2020.1854244>



© 2021 The Author(s). Published by Informa UK Limited, trading as Taylor & Francis Group.



[View supplementary material](#)



Published online: 02 Feb 2021.



[Submit your article to this journal](#)



Article views: 1731



[View related articles](#)



[View Crossmark data](#)



Citing articles: 1 [View citing articles](#)

RESEARCH PAPER



## Discovery of new non-pyrimidine scaffolds as *Plasmodium falciparum* DHFR inhibitors by fragment-based screening

Marie Hoarau, Jarunee Vanichtanankul, Nitipol Srimongkolpithak, Danoo Vitsupakorn, Yongyuth Yuthavong and Sumalee Kamchonwongpaisan

National Center for Genetic Engineering and Biotechnology (BIOTEC), National Science and Technology Development Agency, Pathumthani, Thailand

### ABSTRACT

In various malaria-endemic regions, the appearance of resistance has precluded the use of pyrimidine-based antifolate drugs. Here, a three-step fragment screening was used to identify new non-pyrimidine *Plasmodium falciparum* dihydrofolate reductase (*Pf*DHFR) inhibitors. Starting from a 1163-fragment commercial library, a two-step differential scanning fluorimetry screen identified 75 primary fragment hits. Subsequent enzyme inhibition assay identified 11 fragments displaying  $IC_{50}$  in the 28–695  $\mu$ M range and selectivity for *Pf*DHFR. In addition to the known pyrimidine, three new anti-*Pf*DHFR chemotypes were identified. Fragments from each chemotype were successfully co-crystallized with *Pf*DHFR, revealing a binding in the active site, in the vicinity of catalytic residues, which was confirmed by molecular docking on all fragment hits. Finally, comparison with similar non-hit fragments provides preliminary input on available growth vectors for future drug development.

### ARTICLE HISTORY

Received 28 September 2020  
Revised 8 November 2020  
Accepted 17 November 2020

### KEYWORDS

Malaria; *Plasmodium falciparum*; fragment-based screening; dihydrofolate reductase; small molecule inhibitors

### Introduction

In the fight against malaria, antifolates were once regarded as safe, efficient drugs against the *Plasmodium spp.* parasite. However, the appearance of resistance-inducing mutations in the folate biosynthesis enzymes such as dihydrofolate reductase (DHFR) and dihydropteroate synthase (DHPS) in the parasite has precluded the use of the existing antifolate drugs<sup>1</sup>. Although the recent anti-malarial drugs are geared towards exploiting different drug targets, such as P-type  $Na^+$ -ATPases transporter (*Pf*ATP4), V-type  $H^+$ -ATPase transporter, Phosphatidylinositol 4-kinase (*Pf*I4K) or dihydroorotate dehydrogenase (*Pf*DHODH)<sup>2</sup>, *Pf*DHFR remains attractive in light of the fact that known three-dimensional structures enable rational drug design against the WT and mutant parasite strains<sup>3–5</sup>.


Historically, antifolates have been developed by mimicking the enzymes natural substrates. As such, the two DHFR-targeting drugs pyrimethamine (**PYR**) and cycloguanil (**CYC**) share a similar 2,4-diamino pyrimidine/triazine scaffold mimicking the 2-amino 4-oxo-pteridine core of DHF (Figure 1(A)). A series of *Pf*DHFR co-crystal structures with antifolate derivatives (e.g., PDB 3QGT<sup>6</sup>, 3UM8<sup>7</sup>, 1J3K<sup>4</sup>, 4DP3<sup>8</sup>) generated by our team have enabled elucidation of the role of each functional group in ligand binding (Figure 1). This combination of interactions makes of these antifolates excellent WT *Pf*DHFR inhibitors, with  $K_i$  in the (sub-) nanomolar range. However, their efficiency dramatically decreases against *Pf*DHFR variants carrying S108N mutation such as the double mutant (DM) (C59R + S108N) and quadruple mutant (QM)

(DM + N511 + I164L) *Pf*DHFR due to steric clash of the *p*Cl-phenyl of **PYR** and **CYC** with S108N<sup>4</sup>.

In 2012, our group discovered the compound **P218** which displays nanomolar range *in vitro* activities for *P. falciparum* strains carrying WT and QM *Pf*DHFR<sup>8</sup>. The compound was recently found to display favourable safety, tolerability and pharmacokinetics in first-in-human clinical trial<sup>9</sup>. **P218** was developed through the combination of the 2,4-diaminopyrimidine moiety, with a flexible linker carrying a phenyl ethylcarboxylate group, taking advantage of the conserved R122 to give **P218** a second distant anchoring point (Figure 1(A)). The design of **P218** demonstrated the utility of new chemotypes to target specific residues in the *Pf*DHFR active site. By combining a careful deconstruction of long-known inhibitors with the incorporation of new chemotypes, it became possible to develop new-generation antifolates that by-pass the drug resistance hurdle.

In the last decade, the fragment-based screening (FBS) strategy has emerged as a powerful method to identify new chemotypes for drug discovery and development. Techniques used in FBS, which typically include differential scanning fluorimetry (DSF), surface plasmon resonance (SPR), NMR and X-ray crystallography<sup>10,11</sup> are simple, robust and reproducible. FBS strength resides in an efficient sampling of the chemical space, as even small fragment libraries can encompass high levels of diversity. Interactions between fragment hits and their protein targets are also of higher quality, which eases downstream lead molecule development and optimisation. For these reasons, FBS is widely used in both pharmaceutical industry and academia<sup>10</sup>. Although it has been

**CONTACT** Marie Hoarau  [sumaleek@biotec.or.th](mailto:sumaleek@biotec.or.th)  [marie.hoa@ncr.nstda.or.th](mailto:marie.hoa@ncr.nstda.or.th)  National Center for Genetic Engineering and Biotechnology (BIOTEC), National Science and Technology Development Agency, Pathumthani, 12120, Thailand

 Supplementary data for this article can be accessed [here](#).

© 2021 The Author(s). Published by Informa UK Limited, trading as Taylor & Francis Group.

This is an Open Access article distributed under the terms of the Creative Commons Attribution-NonCommercial License (<http://creativecommons.org/licenses/by-nc/4.0/>), which permits unrestricted non-commercial use, distribution, and reproduction in any medium, provided the original work is properly cited.

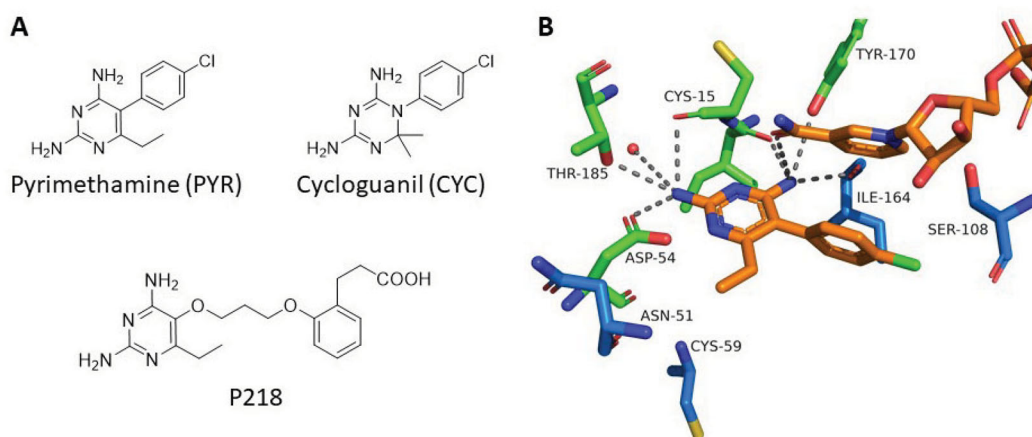


**Figure 1.** (A) Structure of some *Plasmodium* antipfolates. (B) Binding mode of PYR in WT PfDHFR (PDB 3QGT). Resistance-induced mutated residues appear in blue.

successfully applied to other infectious diseases<sup>12–16</sup>, FBS has only been scarcely used against malaria drug targets<sup>17,18</sup>.

Following this idea, we have employed the FBS strategy to identify new chemotypes for inhibitor development against WT PfDHFR. Upon PYR and CYC drug pressure, multiple mutations of PfDHFR have appeared to preclude the binding of these inhibitors, decreasing their binding affinity for QM by several hundred to thousand folds as compared to WT. Several examples have shown that, using the same chemotypes, new inhibitors (such as *m*-Cl derivatives of PYR and CYC, WR99210 and P218) could be rationally designed to avoid steric clash with S108N and display similar binding affinity for WT and QM enzymes<sup>4,8,19–21</sup>. Following this idea, we proposed to identify new active fragments that could interact with both WT and QM. Using WT PfDHFR has practical advantages, as it is more stable, well-characterised, and easier to target with low-affinity fragments compared to the mutant enzymes. For these reasons, we chose to focus our efforts on the fragment-based high-throughput screening of WT PfDHFR. Once the fragment hits identified and characterised, the structural specificities of both WT and QM variants can be integrated in the drug design process, using the extensive structural information available to design larger drug candidates<sup>4,6–8</sup>.

Here, a commercial fragment library was screened using differential scanning fluorimetry (DSF) and fragment hits were further validated by enzymatic assay and X-ray crystallography to identify several active fragments against WT PfDHFR.

## Materials and methods

### Chemicals

SYPRO Orange was purchased from Invitrogen and PYR and NADPH were purchased from Sigma Aldrich. DHA<sup>22</sup>, P218<sup>8</sup>, P30<sup>23</sup>, P45<sup>19</sup>, P24<sup>23</sup>, L4<sup>8</sup> and L5 (manuscript in preparation) were synthesised following previously described procedures. Compounds were numbered as follows: the P series corresponds to previously reported PfDHFR inhibitor prototypes developed by our group. The L compounds are reaction intermediates that were used here as controls. Commercial fragments were numbered following the random order provided by the supplier.

### Fragment library selection and preparation

The BIONET Premium fragment library was purchased from Key Organics, containing 1163 fragments. Fragments were received as

dried powder/oils, and stock solutions were prepared by dissolving *ca.* 3 mg in DMSO to 200 mM. For primary screening, quadruplex fragment mixtures were prepared by mixing equal volumes of four fragments, providing 50 mM solutions. For secondary screening of hit mixtures, individual fragment solutions were prepared by four-fold dilutions of the 200 mM stock in DMSO. For fragment hits, pK<sub>a</sub> values were predicted using MarvinSketch 20.13.

### Protein expression and purification

PfDHFR and HsDHFR expression was completed following a previously published procedure<sup>24</sup>. In brief, *E. coli* BL21(DE3) pLysS cells carrying the plasmid encoding for WT-PfDHFR and HsDHFR, respectively, were grown at 37 °C until reaching an OD<sub>600</sub> *ca.* 0.8. Protein expression was induced by addition of 0.4 mM IPTG and cells were cultured overnight at 20 °C. Cells were harvested and cell pellet was stored at –20 °C. For purification, cells were thawed on ice and lysed by French Press. Lysate was then clarified by centrifugation and applied to a methotrexate (MTX) affinity column. The column was washed overnight, and protein was eluted using dihydrofolate (DHF). In a second purification step, protein was concentrated and applied to a Q-Sepharose ion-exchange column. Protein was eluted using a gradient of KCl. Fractions containing protein were concentrated and their purity was assessed by SDS-PAGE. Protein concentration was measured using Bradford assay.

### Differential scanning fluorimetry

Prior to screening, DSF parameters such as protein and SYPRO Orange concentration, and buffer composition and heating rate were optimised to give the best-defined thermal denaturation peak. The most suitable conditions were found to be 10 μM PfDHFR, 8x SYPRO Orange in Phosphate buffer pH 7.2 20 mM containing 50 mM KCl, 0.1 mM EDTA and 20% glycerol.

In a typical DSF experiment, a master mix containing buffer, PfDHFR and 8x SYPRO Orange dye were prepared in a microcentrifuge tube. Ligands of interest were dispensed in low-profile 96-well plates (Bio-Rad) to 1 mM final concentration, and the master mix was dispensed to a final volume of 50 μL per well. In these conditions, DMSO content was maintained constant at 2%. The microplate was sealed with adhesive film and mixed by shaking for 2 min at 800 rpm at RT. The microplate was then submitted to a DSF run on a CFX96 RT-PCR (Bio-Rad). DSF program was

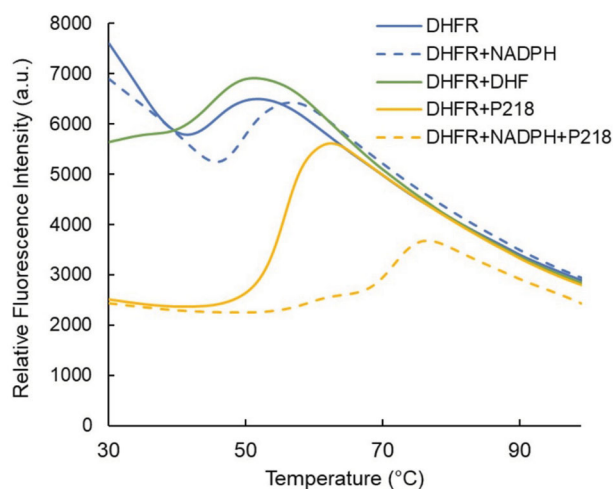


**Figure 2.** DSF curves obtained for *PfDHFR* in the presence of its substrate, cofactor, and **P218** inhibitor.

designed by starting with a 3 min equilibration phase at 30 °C, followed by a temperature gradient of 1 °C/min, recording fluorescence every 0.5 °C. Fluorescence was recorded using the FRET channel ( $\lambda_{exc} = 450\text{--}490\text{ nm}$ ,  $\lambda_{em} = 560\text{--}580\text{ nm}$ ). Curves were fitted using the Precision Melt Analysis software (Bio-Rad).

For the primary screening, DSF chromatograms were recorded for *PfDHFR* in the presence of quadruplex fragment mixtures containing 4 fragments at 50 mM each. The experiment was set as described above, using 1  $\mu\text{L}$  quadruplex mixtures in a final volume of 50  $\mu\text{L}$  (1 mM final fragment concentration). For each experiment, a DMSO negative control was included. Every experiment was run in triplicate and the average  $\Delta T_m$  was considered. The standard deviation of the negative control was calculated and a threshold of twice the standard deviation was applied to define hits.

For secondary screening of each hit mixture obtained from the quadruplex screen, individual fragment stocks were prepared to a final concentration of 50 mM in DMSO. DSF experiments were then run for each individual fragment as described above. For fragments displaying a significant  $\Delta T_m$ , the experiment was run in triplicate. The standard deviation of the negative control was calculated and a threshold of twice the standard deviation was applied to define hits.

### **PfDHFR activity assay**

*PfDHFR* activity was assessed following a previously published procedure<sup>24</sup>. In brief, a master mix was prepared by mixing DHF and NADPH in activity buffer (Tris pH 7.2 50 mM,  $\beta$ -mercaptoethanol 75 mM, BSA 1 mg/mL) to a final concentration of 100  $\mu\text{M}$ . In a 96-well plate, 2  $\mu\text{L}$  of fragments in DMSO were dispensed, followed by 178  $\mu\text{L}$  of the master mix. The reaction was initiated by addition of 20  $\mu\text{L}$  of enzyme followed by immediate mixing. NADPH consumption was monitored by recording absorbance at 340 nm for 80 s. Curve was fitted using a linear regression function and % activity was calculated by comparison with a DMSO control. For  $\text{IC}_{50}$  determination, data points corresponding to variable inhibitor concentrations were plotted in a semi-logarithmic scale, and curve was fitted using the Hill equation.

### **Molecular docking**

Molecular docking experiments were conducted using Autodock 4 program. PDB file 3QGT was edited to remove water molecules

and co-crystallized **PYR** ligand. The protein receptor file was then generated using Autodock Tools 1.5.6. Ligand files were obtained by drawing 2D structure using ChemDraw software, and 3D structure was built and energy-minimized using Avogadro software Universal Force Field. Area of interest was defined using a grid encompassing the pterin binding pocket of the *PfDHFR* active site. Rigid molecular docking was performed using Autodock 4<sup>25</sup> using default parameters. Results were processed by clustering data and considering the lowest energy cluster and/or the most populated cluster. Structural graphics were drawn with PyMOL<sup>26</sup>.

### **X-ray crystallography**

Co-crystallization of purified WT *PfDHFR*-TS (15 mg/mL) with 2–5 mM each of the compound of interest, NADPH and dUMP was performed using a previously published procedure [4]. Data were collected using SC XRD series: D8 venture Bruker at NSTDA Characterisation and Testing Service Centre (NCTC). Data were processed using PROTEUM3 software. Structure model was built by MOLREP<sup>27</sup>, using PDB 1J3I as a template and refined by REFMAC5<sup>28</sup> in CCP4. The model building was done using COOT<sup>29</sup>. Structural graphics were drawn with PyMOL<sup>26</sup>. Co-crystal structures with fragments **263**, **820** and **148** were deposited in the PDB database under accession numbers 7CTY, 7CTW and 7CTZ.

## **Results**

### **Validation of DSF for *PfDHFR* inhibitor screening**

Among the available primary fragment screening methods, DSF was selected for its low cost and ease of use<sup>30</sup>. In order to validate its efficacy to detect *PfDHFR* binders, DSF was first tested on DHFR substrates, as well as a series of known inhibitors. While dihydrofolate (DHF), and tetrahydrofolate (THF) showed minor melting temperature variations, NADPH showed a notable +4 °C stabilisation (Figure 2). This result was further confirmed in the presence of inhibitors. When tested on the apo *PfDHFR*, the **P218** inhibitor displayed a +10 °C stabilising effect. This effect increases to +23.1 °C in the presence of NADPH. The same effect is observed with other pyrimidine-based inhibitors and confirms that NADPH is needed to pre-organize the pterin binding site, so that inhibitors can bind in their most favourable configuration, as reported for DHFR from other organisms<sup>31,32</sup>.

As a preliminary assessment of DSF for *PfDHFR* ligand detection, *PfDHFR* inhibitors displaying variable activity were assayed in the presence of NADPH. All inhibitors displayed measurable  $\Delta T_m$ , except for **L5** (synthetic precursor of the 2,4-diaminopyrimidine series). Dihydroartemisinin (DHA) was added as a negative control, as an antimalarial that does not target folate biosynthesis enzymes.  $\Delta T_m$  results obtained for the different inhibitors appear in Figure 3. Although the correlation between the  $\Delta T_m$  and the  $K_i$  values is not strictly linear ( $r^2 = 0.756$ , Figure 3(B)), a consistent trend is observed. This is consistent with the complex nature of inhibitor binding, as the sum of variable enthalpic vs. entropic contributions that results in an apparent stabilising/destabilising effect<sup>33</sup>. In this view, it is interesting to note that when comparing **P218** and **PYR**, the presence of the carboxylate chelating group does not involve a drastic change of  $K_i$ , while a strong structure stabilising effect is observed by DSF with  $\Delta T_m$  of 23.1 vs 15.1 °C for **P218** and **PYR**, respectively. The technique also shows sensitivity to small structural changes in the pyrimidine-based inhibitor series. This result demonstrates the ability of DSF to detect fragments with a  $K_i$  as high as micromolar (**L4**). However, as  $\Delta T_m$  is a

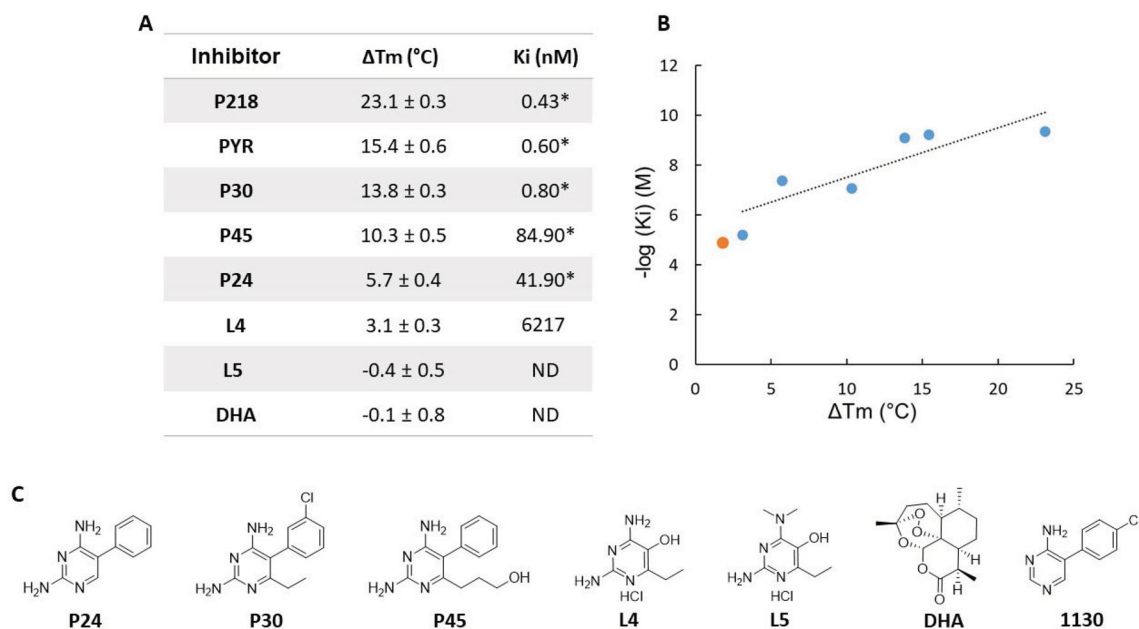


**Figure 3.** (A)  $\Delta T_m$  and inhibition constants of the different inhibitors tested. Data noted \* are from<sup>8,19</sup>. (B) Correlation between  $\Delta T_m$  and inhibition constants of the inhibitors (blue). Linear trendline appears as black dashed line ( $r^2 = 0.756$ ). Fragment 1130 (orange) was added for comparison. (C) Structure of the inhibitors. ND: Not detected.

function of the enthalpic vs. entropic nature of the binding, and  $K_i$  represents completion in binding between substrate and inhibitor, one cannot extrapolate this to all chemotypes<sup>33</sup>.

### Fragment library screening

A DSF primary screening of *Pf*DHFR was undertaken using the BIONET Premium library containing 1163 fragments. This library was chosen over other commercial ones as it is rule-of-three compliant and was curated from any PAINS and aggregating compounds. All fragments are also soluble at 200 mM in DMSO and display high diversity.

Fragments were first screened against *Pf*DHFR as mixtures of 4 at 1 mM in the presence of NADPH (Figure 4(A)). In these conditions, a  $T_m$  of  $47.26 \pm 0.4^{\circ}\text{C}$  was measured for *Pf*DHFR in the presence of DMSO as a control. Considering the multiple thermodynamic factors influencing the  $\Delta T_m$ , it seems virtually impossible to apply a definitive threshold that would encompass all potential fragment binders. We thus decided, as others before us, to consider our hit threshold as twice the standard deviation of the DMSO control, relying on the experimental technique limitations. Fragments were thus considered as hits when their individual  $\Delta T_m$  exceeded  $\pm 0.8^{\circ}\text{C}$ . Out of 291 quadruplex mixtures tested, 87 exceeded the set criterion, with  $\Delta T_m$  ranging from  $-7.66^{\circ}\text{C}$  to  $+6.5^{\circ}\text{C}$ . The fragments composing these mixtures were thus examined individually, affording a total of 75 fragment hits (6.4% hit rate) with  $\Delta T_m$  spanning between  $-12.5^{\circ}\text{C}$  and  $+5.2^{\circ}\text{C}$  (Figure 4(B)). Among these, 14 fragments displayed a negative  $T_m$ . The overall 6.4% hit rate matches the results obtained in typical fragment screening campaigns.

In order to validate these primary hits, the 75 primary fragment hits were subjected to a DHFR inhibition assay. As shown in Figure 5, 11 fragments displayed 43–95% *Pf*DHFR inhibition at 500  $\mu\text{M}$  (i.e., 0.8% of the library). These fragments were grouped by tentative chemotypes.

The fragment hits found display  $\text{IC}_{50}$  values in the 28 – 695  $\mu\text{M}$  range. Among the 11 active fragments, 5 were found to inhibit

WT *Pf*DHFR with 78 – 84% inhibition at 500  $\mu\text{M}$ , with corresponding  $\text{IC}_{50}$  values of 28 – 156  $\mu\text{M}$ . Fragment **263** exhibited the best overall inhibition, while fragment **1130** showed the best inhibition at 500  $\mu\text{M}$ . Little correlation was observed between the  $\Delta T_m$  and the ability to inhibit the enzyme ( $r^2 = 0.41$ ). As such, fragments **80**, **148** and **218** all display a  $\Delta T_m$  of  $0.83^{\circ}\text{C}$ , close to the limit of detection, while showing enzyme inhibition varying by several folds ( $\text{IC}_{50}$  *Pf*DHFR of 258, 464 and 695  $\mu\text{M}$ , respectively). All the active fragment hits display a positive  $\Delta T_m$ . In order to evaluate enzyme selectivity, inhibition of the *Homo sapiens* (*Hs*) DHFR was also measured for the 11 active hits in the same conditions. All fragments were found inactive against *Hs*DHFR, showing overall selectivity for the *Pf* enzyme (Figure 5(B)).

Fragment **1130** (5-(4-chlorophenyl)pyrimidin-4-amine) is the only compound related to the 2,4-diaminopyrimidine-based antifolate series. Its core structure relates to **PYR** but lacks one aromatic amino group and the 6-ethyl side substituent. Our previous work demonstrated that these groups are necessary to promote direct interaction with the protein, through Cys15, Asp54 and Thr185 (Figure 1)<sup>8</sup>. The absence of these two groups in **1130** results in a loss of affinity by four orders of magnitude compared to **PYR**, in line with our DSF results (Figure 3). In addition, it should be noted that in a retrosynthetic approach, fragments **L4** and **1130** complement each other into **PYR**. This illustrates the end goal of fragment-based drug discovery in which the merging of medium affinity fragments leads to a compound with dramatically improved affinity<sup>34,35</sup>. This result also suggests that the *p*-Cl phenyl ring (present in **1130**) and the amino and ethyl substituents (present in **L4**) equally contribute to the high binding affinity of **PYR**.

The main chemotype unravelled by this screening was defined as bicyclic fragments with a heteroalkyl cyclic ring, a linker, and a phenyl ring with or without substituent. This group includes four 4-phenyl-piperidines (fragments **132**, **240**, **263**, and **813**), four 4-phenyl-piperazines (fragments **218**, **800**, **820** and **1157**), and one phenyl-pyrrolidine (fragment **80**). These compounds with high  $\text{pK}_a$  values ( $7.16 < \text{pK}_a < 11.43$ ) are in their protonated form at physiological pH, which might result in poor cell penetration due to

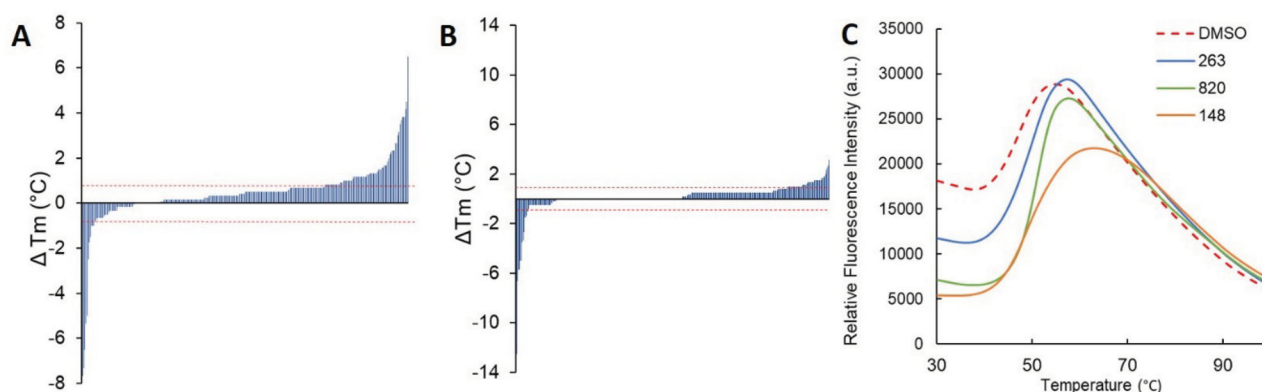


**Figure 4.** Distributions of fragment hits  $\Delta T_m$  for quadruplex mixtures screening (A) and individual fragment screening (B). The  $\pm 0.8^\circ\text{C}$  threshold applied appears as red dashed lines. C. Representative examples of DSF curves obtained.

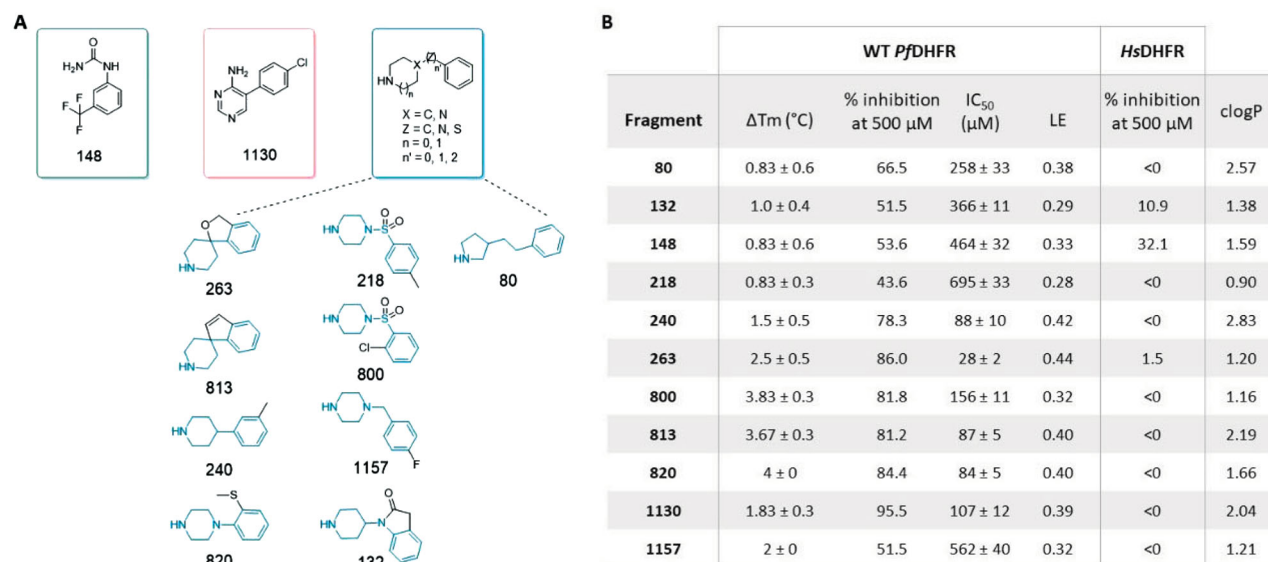


**Figure 5.** (A) Fragment hits structures grouped by tentative chemotypes. (B) Corresponding experimental data obtained for the fragment hits. clogP values were calculated using DataWarrior<sup>43</sup>. LE: Ligand Efficiency.

their positive charge. Fragments **263** and **813** differ by the presence of a fused 5-member ring that rigidifies the system and prevents free rotation of the two rings.

Finally, fragment **148** is the only monocyclic fragment, constituted of a phenyl ring bearing urea and a trifluoromethyl substituents in 1,3 position. It is neutral at physiological pH, which could ease future lead design.

### Crystallography of selected fragments complexed with *PfDHFR-TS*

Three representative active fragments belonging to each chemotype, fragments **148** (phenyl urea), **820** (piperazine) and **263** (piperidine) were selected for co-crystallization with *PfDHFR-TS* (the native bifunctional form of the protein) based on their highest DHFR inhibitory activity at 500  $\mu\text{M}$ . Despite an overall low fragment occupancy, crystal structures were successfully obtained for each complex at resolutions between 2.70–2.85 Å. All crystals showed the expected orthorhombic arrangement ( $P2_12_12_1$ ), with two protein chains per asymmetric unit. All the data collection and refinement statistics appear in Table S1. Very little variation was observed between the protein backbone of three structures (Figure S1).

All three fragments were confirmed to bind into *PfDHFR* active site, occupying the space delimited by Asp54, Phe58, and NADPH normally occupied by the pteridine moiety of DHF. Fragments **263** and **820** display a similar binding mode, with a H-bond mediated interaction with Asp54 (Figure 6(A,B)). As the secondary amines are in their protonated form at physiological pH, the interaction is likely to be strengthened through charge pairing. For the two fragments, the phenyl ring is stacked in the apolar region defined by NADPH and Phe58, however the ring positioning differs between the two complexes. In **263**, the phenyl ring is positioned 4.7 Å from the NADPH nicotinamide ring and forms a  $\pi$ - $\pi$  interaction, while in **820**, the phenyl ring is coplanar to the Phe58 phenyl ring. This could be the origin of the higher inhibitory potential of fragment **263**, as its binding mode might prevent substrate access to the catalytic Asp54 as well as to the NADPH cofactor.

Due to its similarly sized substituents in 1,3 position of the phenyl ring, the electron density for fragment **148** displays a symmetrical shape that is compatible with two ligand orientations. Because crystallographic evidence did not allow conclusion on a preferred conformation, both were proposed in the crystal structure (Figure 6(C)). In the first conformation, the urea moiety interacts with the protein *via* a double H-bond mediated interaction

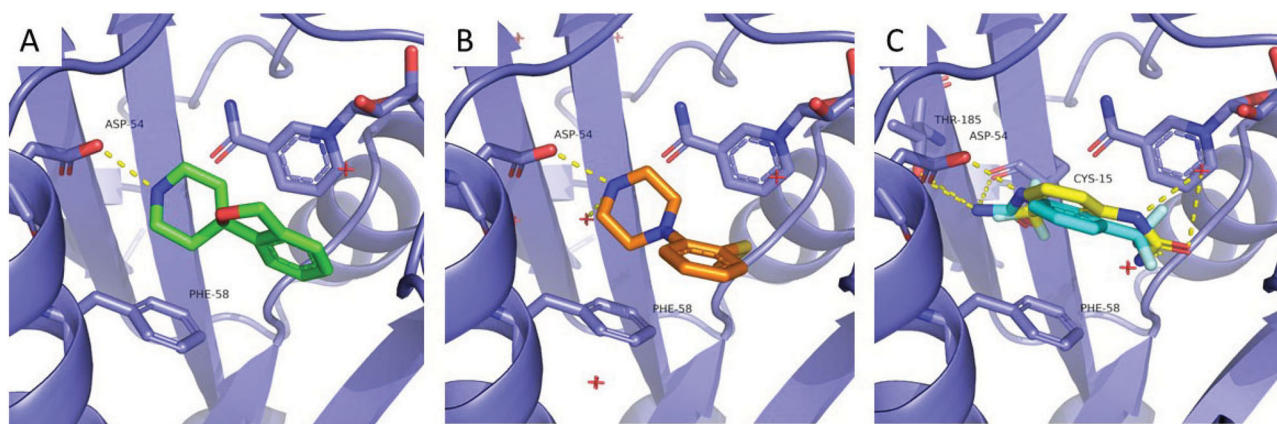


**Figure 6.** Crystal structures for fragment **263** (PDB 7CTY) (A), fragment **820** (PDB 7CTW) (B) and fragment **148** (PDB 7CTZ) in conformation A (cyan) and conformation B (yellow) (C). Interacting residues and NADPH appear as sticks, polar contacts appear as yellow dash lines.

with Asp54. Polar contacts are also observed with Thr185 side chain hydroxy group and Cys15 backbone carbonyl. The phenyl ring is equidistant from Phe58 and nicotinamide ring of NADPH, with the trifluoromethyl substituent pointing towards Ser108. In the second conformation, the trifluoromethyl substituent is facing Asp54 and Cys15, while the urea moiety forms polar contact with Ile164 backbone carbonyl and with a water molecule. The phenyl ring is tilted towards Phe58.

From a strictly chemical perspective, the first conformation would appear as more likely, as the set of interactions observed resembles the interactions of the DHF substrate. However, at this stage, it is not possible to conclude from crystallographic data which conformation is occurring, or if the two binding modes are present simultaneously.

#### Molecular docking analyses of selected fragment hits

As a complement to crystallographic data, molecular docking experiments were conducted to study binding mode variations for all the active fragment hits. The *PfDHFR* structure (PDB 3QGT) was used, from which **PYR** and water molecules were removed, while bound NADPH was conserved, and docking parameters were defined to encompass the whole catalytic pocket. Docking scores and ligand efficiencies (LE), corresponding to the calculated binding energy per non-hydrogen atom, appear in Figure 7(B).

Along the phenyl piperidine/piperazine series, molecular docking suggests a binding mode consistent with the crystal structure obtained for fragments **263** and **820**, with an interaction between the fragment protonated secondary amine and Asp54. Although an important flexibility is conferred by the aliphatic ring, the aromatic rings tend to align with the NADPH nicotinamide ring for all fragments, except for the extended ring of fragment **132** (Figure 7(A) and Figure S2).

The docking pose of fragment **148** is consistent with the first conformation proposed in the crystal structure, with a coordination of the urea to Asp54 via two parallel H-bonds, while the trifluoromethyl substituent is pointing towards Ile164 and Ser108. The phenyl ring is tilted compared to the crystal structure to be coplanar with NADPH. The comparatively low docking score obtained could be attributable to a poor estimation of the trifluoromethyl contribution by the software's scoring function (Figure 7(B)).

Expectedly, molecular docking on fragment **1130** provided a similar binding pose as co-crystallized **PYR**, with a slightly twisted conformation of the rings, possibly due to the absence of

interaction with Asp54 (Figure 7(A)). Its docking score is comparatively lower than for the phenyl piperidine/piperazine derivatives (Figure 7(B)).

## Discussion

### *PfDHFR* fragment-based screening and re-discovery of **PYR** by fragment-based approach

Starting from a 1163 fragments library, our screening workflow enabled us to identify 11 fragments displaying inhibitory activity on WT *PfDHFR*. Compared to other fragment-based screening studies, ours can be considered successful, as it is common to see campaigns yielding fragments that bind their target too weakly to detect any measurable inhibition<sup>34</sup>.

Out of 11 active fragment hits, only one fragment resembles the pyrimidine-based inhibitor series. This constitutes a validation of FBS applied to *PfDHFR*, as FBS would have allowed discovery of **PYR** and **CYC**, if they had not already been developed. More importantly, the fact that besides **1130**, 10 other unrelated fragments showed similar (or better) inhibitory properties confirmed the success of the FBS approach to identify novel anti-*PfDHFR* chemotypes.

### New anti *PfDHFR* chemotypes

Among the fragment hits identified, the largest part is constituted of 4-phenyl-piperidines and 4-phenyl-piperazines. Two successive studies from 2005 and 2012 demonstrated the antimalarial effect of mono- and di-substituted piperazines on both chloroquine-sensitive and resistant *P. falciparum* strains<sup>36,37</sup>. A structure-activity relationship (SAR) study showed that the presence of a free amino group was essential to guarantee the inhibition, prompting the authors to assume of the existence of an unknown protein target. In this study, we provide evidence that both phenyl piperidine and piperazine derivatives target the active site of *PfDHFR*. This is supported by the crystal structure obtained for fragments **820** and **263** showing electron density in the *PfDHFR* active site.

Looking closely at the structure of these fragment hits, and as importantly at the non-hits, allows us to build a preliminary SAR study along this fragment series (Figure S3). Consistently with previous observation<sup>37</sup>, we note that none of the piperazine fragments with protected secondary amine present in the library appeared as a hit by DSF. 2-phenyl piperazine derivatives (*i.e.*, asymmetric piperazines bearing the phenyl ring linked to an aliphatic carbon) were also negative.

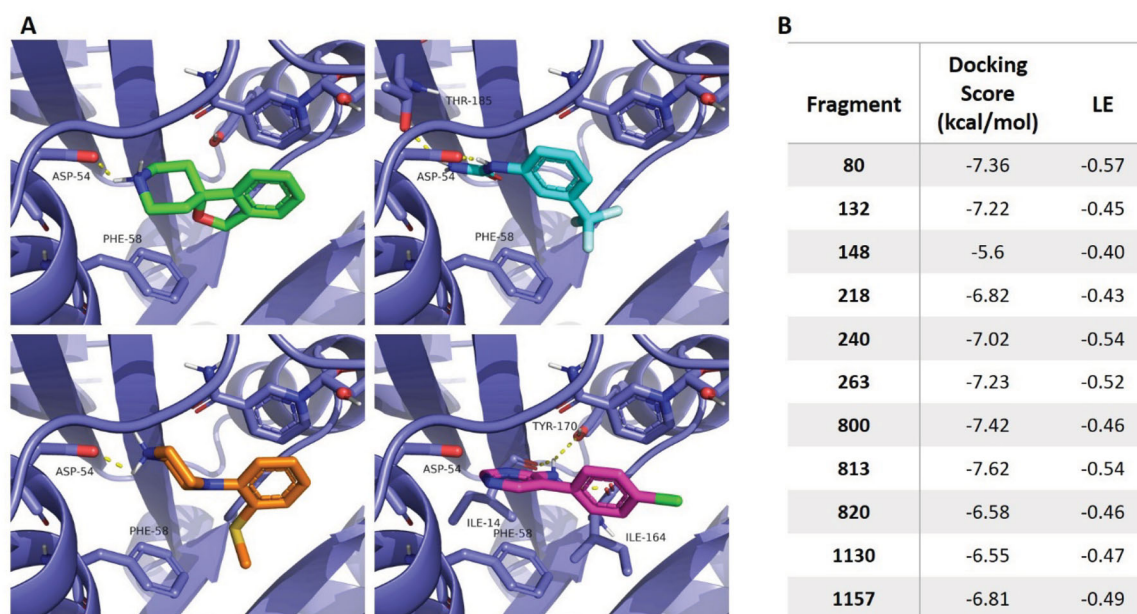


**Figure 7.** (A) Detail of molecular docking results for fragments **263** (green), **820** (orange), **148** (cyan) and **1130** (pink). Interacting residues and NADPH appear as sticks. (B) Corresponding docking scores and ligand efficiencies (LE) for each fragment.

Although hits display variable linker lengths, the shortest ones seem favourable for inhibition. For the piperazines, the introduction of an angle between the rings is also a beneficial feature (fragments **2**, **132**, **263**, **813**), probably promoting a favourable alignment with NADPH. Finally, the nature and position of the phenyl ring substituents seem to be of crucial importance. At this stage, it cannot be concluded whether these variations are due to steric constraints or to a precise tuning of the electronic properties of the phenyl ring, and it seems clear that a more systematic SAR study will be key for future lead development.

A second chemotype identified is the [3-(trifluoromethyl)phenyl]urea (fragment **148**). This is in line with the work from Rastelli *et al.* who identified (thio)urea derivatives as a pharmacophore of interest by computational screen on *PfdHFR*<sup>38</sup>. In their study, *PfdHFR* inhibition was confirmed experimentally for seven derivatives, showing  $K_i$  values in the low  $\mu\text{M}$  range. Here, our fragment-based screening was able to further minimise the chemical group responsible for interaction. Importantly, none of the substituted ureas, either through methylation (fragments **894**, **895**, **959**, **960**) or cyclisation (fragments **361**, **369**), showed any interaction or inhibition towards *PfdHFR* (Figure S4). This supports the first conformation proposed in the crystal structure, showing that the presence of both the primary and the secondary amine are involved in the interaction through two parallel hydrogen bonds and two polar contacts. An equilibrium with the tautomeric form of the urea could also be envisaged.

### Opportunities for lead development

For the two new chemotypes identified in this screening campaign, novel opportunities appear in terms of growth vectors. Using piperidines or piperazines offers a chance to evolve the fragment in three dimensions, taking advantage of the ring flexibility, which cannot be done with the planar 2,4-diaminopyrimidine. This series of fragment hits also accommodates a variety of phenyl ring substituents, enabling functionalization in different directions. The high LE values measured for these fragments make them promising starting points for lead development, provided

that LE can be maintained through the design process. Another important parameter to consider for future drug design is the clogD value. Because they are positively charged at physiological pH, piperazines and piperidines are commonly used to improve drugs water solubility<sup>39,40</sup>. However, this may come with a decrease in cell penetration and/or tissue distribution. Design will have to include a strategy to increase lipophilicity of future lead candidates to reach a suitable clogD range.

The potential of phenyl urea fragment **148** resides in the positioning of its phenyl ring. Because the urea moiety is relatively small, the phenyl ring is positioned about 2 Å deeper into the active site compared to **PYR** and is facing Phe58. This reduces the risk of steric clash with S108N, but also provides an opportunity to target this residue, by incorporation of a suitable functional group. Complete SAR studies will be needed to elucidate the role of the trifluoro substituent. Functionalization in *ortho* or *para* position could also be envisaged, as suggested by the results obtained with fragment **327** (Figure S4).

Another promising feature of these new chemotypes is their selectivity, as they do not show inhibition against *HsDHFR*. This contrasts with the 2,4-diaminopyrimidine-based scaffolds, that do bind *HsDHFR* and for which careful optimisation was necessary to obtain selective compounds. Starting from chemotypes with high selectivity would surely ease the drug design process, although a constant monitoring of selectivity factors should be observed.

Finally, it should be noted that the three active chemotypes identified through this screening were found to bind the enzyme active site, in close proximity with the Asp54 and NADPH. This residue is known to be crucial, both for substrate binding and catalytic activity, and it is not surprising to find that  $\mu\text{M}$ -range binders can impede catalytic activity. However, for portions of the active site with more limited contribution to substrate binding, a  $\mu\text{M}$ -range binding event might not result in detectable inhibition. For this reason, the absence of enzyme inhibition does not make the 64 other fragment hits irrelevant, as they might still bind other portions of the active site, or in other sites. Although this study has focussed on the fragment hits displaying promising inhibitory properties, a complete structural characterisation of the remaining primary fragment hits using X-rays crystallography and



molecular docking would provide valuable information for future design.

## Conclusions

In the context of antifolate resistance, development of new generation antifolates based on novel chemotypes is warranted. Although the fragment-based screening approach has been successfully applied to DHFR enzymes in various bacteria and protozoa<sup>41,42</sup>, no similar study has yet been reported in the malaria parasite *Plasmodium falciparum*. Here, we describe the first fragment-based screening on PfDHFR. In addition to the widely used diaminopyrimidine, three new chemotypes displaying  $\mu\text{M}$ -range PfDHFR inhibition were identified. Most of the 11 active fragment hits showed high selectivity for the target enzyme compared to the human isoform, highlighting the efficiency and specificity of the fragment-based strategy.

The crystal structures obtained for both phenyl piperazine and phenyl urea chemotypes confirm a binding in the enzyme active site, similarly to DHF substrate and pyrimidine-based antifolates. These scaffolds offer new possibilities in terms of growth vectors, enabling exploration of novel regions of the active site. Future work will be devoted to the investigation of these growth vectors through a structure-activity relationship study, paying attention to the selectivity profile towards the antifolate-resistant enzyme variants. These results could pave the way for the discovery of new lead molecules against *P. falciparum* DHFR and give a fresh start to antifolate drug development.

## Acknowledgements

We thank the NSTDA Characterization and Testing Service Center (NCTC) for SC XRD series: D8 venture, and thank Waraporn Pinyo for helping with the D8 Venture system. We thank Netnapa Charoensetakul for the preparation of compounds L4 and L5.

## Disclosure statement

The authors report no conflict of interest.

## Funding

This research was supported by grants from the Medicines for Malaria Venture (MMV), BIOTEC, NSTDA's Cluster and Program Management (P1450883) and NSTDA's Researcher Chair Grant (P1850116).

## References

1. Yuthavong Y, Kamchonwongpaisan S, Leartsakulpanich U, et al. Folate metabolism as a source of molecular targets for antimalarials. *Future Microbiol* 2006;1:113–25.
2. Tse EG, Korsik M, Todd MH. The past, present and future of anti-malarial medicines. *Malar J* 2019;18:93.
3. Yuthavong Y. Basis for antifolate action and resistance in malaria. *Microbes Infect* 2002;4:175–82.
4. Yuvaniyama J, Chitnumsub P, Kamchonwongpaisan S, et al. Insights into antifolate resistance from malarial DHFR-TS structures. *Nat Struct Biol* 2003;10:357–65.
5. Yuthavong Y, Yuvaniyama J, Chitnumsub P, et al. Malarial (*Plasmodium falciparum*) dihydrofolate reductase-thymidylate synthase: structural basis for antifolate resistance and development of effective inhibitors. *Parasitology* 2005;130:249–59.
6. Vanichtanankul J, Taweechai S, Yuvaniyama J, et al. Trypanosomal dihydrofolate reductase reveals natural antifolate resistance. *ACS Chem Biol* 2011;6:905–11.
7. Vanichtanankul J, Taweechai S, Uttamapinant C, et al. Combined spatial limitation around residues 16 and 108 of *Plasmodium falciparum* dihydrofolate reductase explains resistance to cycloguanil. *Antimicrob Agents Chemother* 2012;56:3928–35.
8. Yuthavong Y, Tarnchompoo B, Vilaivan T, et al. Malarial dihydrofolate reductase as a paradigm for drug development against a resistance-compromised target. *Proc Natl Acad Sci USA* 2012;109:16823–8.
9. Chughlay MF, Rossignol E, Donini C, et al. First-in-human clinical trial to assess the safety, tolerability and pharmacokinetics of P218, a novel candidate for malaria chemoprotection. *Br J Clin Pharmacol* 2020;86:1113–24.
10. Erlanson DA, de Esch IJP, Jahnke W, et al. Fragment-to-Lead Medicinal Chemistry Publications in 2018. *J Med Chem* 2020;63:4430–44.
11. Bancet A, Raingeval C, Lomberget T, et al. Fragment linking strategies for structure-based drug design. *J Med Chem* 2020;63:11420–35.
12. Chhabra S, Dolezal O, Hattarki M, et al. Fragment screening on *Staphylococcus aureus* HPPK – a folate pathway target. *Aust J Chem* 2013;66:1537–43.
13. Benmansour F, Trist I, Coutard B, et al. Discovery of novel dengue virus NS5 methyltransferase non-nucleoside inhibitors by fragment-based drug design. *Eur J Med Chem* 2017;125:865–80.
14. Christopheit T, Leiros H-KS. Fragment-based discovery of inhibitor scaffolds targeting the metallo- $\beta$ -lactamases NDM-1 and VIM-2. *Bioorg Med Chem Lett* 2016;26:1973–7.
15. Hudson SA, McLean KJ, Surade S, et al. Application of fragment screening and merging to the discovery of inhibitors of the mycobacterium tuberculosis cytochrome P450 CYP121. *Angew Chem Int Ed Engl* 2012;51:9311–6.
16. Liu M, Quinn RJ. Fragment-based screening with natural products for novel anti-parasitic disease drug discovery. *Expert Opin Drug Discov* 2019;14:1283–95.
17. Vu H, Roullier C, Campitelli M, et al. Plasmodium gametocyte inhibition identified from a natural-product-based fragment library. *ACS Chem Biol* 2013;8:2654–9.
18. Vu H, Pedro L, Mak T, et al. Fragment-based screening of a natural product library against 62 potential malaria drug targets employing native mass spectrometry. *ACS Infect Dis* 2018;4:431–44.
19. Kamchonwongpaisan S, Quarrell R, Charoensetakul N, et al. Inhibitors of multiple mutants of *Plasmodium falciparum* dihydrofolate reductase and their antimalarial activities. *J Med Chem* 2004;47:673–80.
20. Saepua S, Sadorn K, Vanichtanankul J, et al. 6-Hydrophobic aromatic substituent pyrimethamine analogues as potential antimalarials for pyrimethamine-resistant *Plasmodium falciparum*. *Bioorg Med Chem* 2019;27:115158.
21. Kamchonwongpaisan S, Charoensetakul N, Srisuwannaket C, et al. Flexible diaminodihydrotriazine inhibitors of *Plasmodium falciparum* dihydrofolate reductase: binding strengths, modes of binding and their antimalarial activities. *Eur J Med Chem* 2020;195:112263.

22. Liu Y, Cui K, Lu W, et al. Synthesis and antimalarial activity of novel dihydro-artemisinin derivatives. *Molecules* 2011;16:4527–38.
23. Tarnchompoo B, Sirichaiwat C, Phupong W, et al. Development of 2,4-diaminopyrimidines as antimalarials based on inhibition of the S108N and C59R+S108N mutants of dihydrofolate reductase from pyrimethamine-resistant *Plasmodium falciparum*. *J Med Chem* 2002;45:1244–52.
24. Chitnumsub P, Yavaniyama J, Vanichtanankul J, et al. Characterization, crystallization and preliminary X-ray analysis of bifunctional dihydrofolate reductase-thymidylate synthase from *Plasmodium falciparum*. *Acta Crystallogr D Biol Crystallogr* 2004;60:780–3.
25. Morris GM, Huey R, Lindstrom W, et al. AutoDock4 and AutoDockTools4: automated docking with selective receptor flexibility. *J Comput Chem* 2009;30:2785–91.
26. The PyMOL Molecular Graphics System, Version 2.4.1 Schrödinger, LLC; 2010.
27. Vagin A, Teplyakov A. Molecular replacement with MOLREP. *Acta Crystallogr D Biol Crystallogr* 2010;66:22–5.
28. Murshudov GN, Skubák P, Lebedev AA, et al. REFMAC5 for the refinement of macromolecular crystal structures. *Acta Crystallogr D Biol Crystallogr* 2011;67:355–67.
29. Emsley P, Lohkamp B, Scott WG, et al. Features and development of Coot. *Acta Crystallogr D Biol Crystallogr* 2010;66:486–501.
30. Mortenson PN, Erlanson DA, de Esch IJP, et al. Fragment-to-Lead Medicinal Chemistry Publications in 2017: miniperspective. *J Med Chem* 2019;62:3857–72.
31. Sawaya MR, Kraut J. Loop and subdomain movements in the mechanism of *Escherichia coli* dihydrofolate reductase: crystallographic evidence. *Biochemistry* 1997;36:586–603.
32. Rod TH, Radkiewicz JL, Brooks CL. Correlated motion and the effect of distal mutations in dihydrofolate reductase. *Proc Natl Acad Sci USA* 2003;100:6980–5.
33. Simeonov A. Recent developments in the use of differential scanning fluorometry in protein and small molecule discovery and characterization. *Expert Opin Drug Discov* 2013;8:1071–82.
34. van Montfort RLM, Workman P, Lamoree B, et al. Current perspectives in fragment-based lead discovery (FBLD). *Essays Biochem* 2017;61:453–64.
35. Murray CW, Rees DC. Opportunity knocks: organic chemistry for fragment-based drug discovery (FBDD). *Angew Chem Int Ed Engl* 2016;55:488–92.
36. Molyneaux C-A, Krugliak M, Ginsburg H, et al. Arylpiperazines displaying preferential potency against chloroquine-resistant strains of the malaria parasite *Plasmodium falciparum*. *Biochem Pharmacol* 2005;71:61–8.
37. Ibezim E, Duchowicz PR, Ortiz EV, et al. QSAR on aryl-piperazine derivatives with activity on malaria. *Chemom Intell Lab Syst* 2012;110:81–8.
38. Rastelli G, Pacchioni S, Sirawaraporn W, et al. Docking and database screening reveal new classes of *Plasmodium falciparum* dihydrofolate reductase inhibitors. *J Med Chem* 2003;46:2834–45.
39. Walker MA. Novel tactics for designing water-soluble molecules in drug discovery. *Expert Opin Drug Discov* 2014;9:1421–33.
40. Rathi AK, Syed R, Shin H-S, et al. Piperazine derivatives for therapeutic use: a patent review (2010-present). *Expert Opin Ther Pat* 2016;26:777–97.
41. Shelke RU, Degani MS, Raju A, et al. Fragment discovery for the design of nitrogen heterocycles as *Mycobacterium tuberculosis* dihydrofolate reductase inhibitors. *Arch Pharm (Weinheim)* 2016;349:602–13.
42. Ruiz V, Czyzyk DJ, Valhondo M, et al. Novel allosteric covalent inhibitors of bifunctional *Cryptosporidium hominis* TS-DHFR from parasitic protozoa identified by virtual screening. *Bioorg Med Chem Lett* 2019;29:1413–8.
43. Sander T, Freyss J, von Korff M, et al. DataWarrior: an open-source program for chemistry aware data visualization and analysis. *J Chem Inf Model* 2015;55:460–73.